

Microscopic model analyses of proton scattering from ^{12}C , ^{20}Ne , ^{24}Mg , ^{28}Si and ^{40}Ca

Y. J. Kim*

Department of Physics, Cheju National University, Jeju 690-756, Republic of Korea

K. Amos†

School of Physics, The University of Melbourne, Victoria 3010, Australia

S. Karataglidis‡

*Department of Physics and Electronics,
Rhodes University, Grahamstown 6140, South Africa*

W. A. Richter§

*Department of Physics, University of the Western Cape,
Private Bag X17, Bellville 7530, South Africa,*

(Dated: February 2, 2008)

Abstract

Differential cross sections and analyzing powers for elastic scattering from, and for inelastic proton scattering to a set of 2_1^+ states in, ^{12}C , ^{20}Ne , ^{24}Mg , ^{28}Si and ^{40}Ca , and for a set of energies between 35 to 250 MeV, have been analyzed. A g -folding model has been used to determine optical potentials and a microscopic distorted wave approximation taken to analyze the inelastic data. The effective nucleon-nucleon interactions used to specify the optical potentials have also been used as the transition operators in the inelastic scattering processes. Shell and large space Hartree-Fock models of structure have been used to describe the nuclear states.

PACS numbers: 21.10.Hw, 25.30.Dh, 25.40.Ep, 25.80.Ek

*Electronic address: yjkim@cheju.ac.kr

†Electronic address: amos@physics.unimelb.edu.au

‡Electronic address: S.Karataglidis@ru.ac.za

§Electronic address: richter@sun.ac.za

I. INTRODUCTION

Proton scattering is a most useful means to study both macroscopic and microscopic aspects of nuclear structure especially now that a coordinate space model analysis of proton-nucleus scattering has been established as a pertinent means to analyze scattering data from most stable nuclei and for energies in the range ~ 30 to ~ 300 MeV. The model as used currently [1] enables predictions to be made of differential cross sections as well as of spin observables. When good models of structure are used, those predictions agree well with data [1]. Using the relative motion wave functions so found as distorted waves in a distorted wave approximation (DWA) for inelastic scattering, predictions have been made that also agree well with observed results. Again that is so when good prescriptions of the structure for the inelastic transitions is used.

Elastic scattering, the predominant event caused by the interactions of nucleons with nuclei, has been studied extensively over many decades. Invariably data are compared with results calculated from optical potentials. All formulations of the nuclear optical model have in common an allowance of flux loss from the incident beam to non-elastic channels when energies are above reaction thresholds. By far the most common approach has been phenomenological with a local, parameterized, potential. Customarily that is of Woods-Saxon form. Much effort has gone into establishing energy and mass dependences of the parameter values with which good fits to data are found. Such a process though has hidden dangers when a physical interpretation is sought for the potentials, and especially when the associated relative motion wave functions through the nuclear volume are used in a DWA to study non-elastic reactions. First, fits to elastic scattering data require definition of an appropriate set of phase shifts which only require solutions of the partial wave Schrödinger equations with the optical potentials to be defined reasonably asymptotically, i.e. at very large distances from the nucleus. Such do not test the credibility of the wave functions through and near to the nucleus itself. Second, all phenomenological potentials inherently support spurious states which, in the actual nucleus, are either Pauli blocked or hindered. Such can be simply ignored unless the local interactions form part of a coupled-channel problem. Then the violation of the Pauli principle has most serious consequences [2, 3]. Third, due to the indistinguishability of the nucleons, knock-out processes exist, where the detected nucleon is not the incident one. This property (also of the Pauli principle) make a nucleon-nucleus (NA) optical potential very non-local. The relative wave functions found from non-local potentials and those obtained from any local form that is phase equivalent are very different. Finally, only with allowance of such non-locality can the determined interaction be related to structure properties of the target. At the least the optical potentials reflect the full one-body density matrix elements (OBDM) of the nuclear states and not just the matter densities of the targets. Similar concerns exist with many calculations of inelastic scattering reported in the literature. Those failing to allow for the exchange scattering amplitudes, which includes almost all coupled-channel calculations built upon collective models, can only achieve the momentum transfer variations seen in data by judicious manipulation of parameter values. Such, by the commission of a violation of the Pauli principle, have no true physical significance.

An objective of NA data analyses, and undoubtably the prime one, is to use the calculated results in comparison with data to assess the quality of the nuclear structure model assumed. Additionally one hopes to identify mismatches and to understand why they occur. To achieve those hopes, the reaction model used must be as sophisticated as the structure one to be

tested. The Pauli principle must be preserved and its prime consequences evaluated as fully as possible. Those of the g -folding and DWA methods in current use [1, 4, 5] seem appropriate to the task. With them, analyses of data from the scattering of radioactive Helium ions from hydrogen [4] showed that ${}^6\text{He}$ has an extended neutron distribution that has been called a neutron halo while ${}^8\text{He}$ has just a skin of neutrons. Likewise, on using detailed structure models of ${}^{208}\text{Pb}$, the g -folding methods revealed [5] that the nucleus should have a neutron root mean square radius ~ 0.16 fm larger than that for protons, consistent with predictions from evaluations of the neutron equation of state [6].

Microscopic optical potentials built using the g -folding model and with effective nucleon-nucleon (NN) interactions in the nuclear medium, have been used successfully to describe NA elastic scattering of nucleons with energies in the range ~ 30 to ~ 300 MeV and for targets over the whole range of mass [1]. When good nuclear structure details are used in the foldings, no *a posteriori* adjustment to those potentials are required to find a credible match to data. The structure details required are the OBDME, which are to be found from large space nucleon models of the nucleus, and a set of single-particle bound-state wave functions. The latter may be those used in the self-same structure model calculations, or selected from consideration of other properties of the nucleus, such as the root mean square radii or electron scattering form factors.

In this paper, by use of the methods described above, we analyze the differential cross sections and analyzing powers for proton elastic scattering from, and inelastic proton scattering to 2_1^+ excited states in, ${}^{12}\text{C}$, ${}^{20}\text{Ne}$, ${}^{24}\text{Mg}$, ${}^{28}\text{Si}$, and ${}^{40}\text{Ca}$, for a range of energies from 35 to 250 MeV. We use a shell model (SM) [7] and a Skyrme-Hartree-Fock (SHF) model [8, 9] to describe the ground-state structure of these nuclei. The single-particle bound-state wave functions that complete the nuclear density matrices are harmonic oscillator (HO), Woods-Saxon (WS), or as given by the SHF studies [8, 9]. For the inelastic scattering calculations, the no-core shell model was used to define the transition OBDME for the excitation of the 2_1^+ state in ${}^{12}\text{C}$. For 2_1^+ transitions in the sd -shell nuclei, however, only projected Hartree-Fock (PHF) studies [10, 11] have been made in a large enough basis to suit. There is an inconsistency in using SHF wave functions with PHF transition OBDME, but we can only await SHF studies giving excitation spectra and transition OBDME. However, with such structure, good results for electron scattering form factors were found [12].

The DWBA98 computer code of Raynal [13] has been used to evaluate both elastic and inelastic (DWA) scattering observables, in which an effective NN interaction (the Melbourne interaction) can be, and has been, used successfully. The DWBA98 program explicitly evaluates the knock-out (exchange) amplitudes that are a result of the (two-nucleon state) antisymmetry requirement to conserve the Pauli principle.

The paper is arranged as follows. In the next section, for completeness, salient details of microscopic scattering theories to analyze the elastic and inelastic scattering data are given. Also in Sec. II, the structure information required, and determined by diverse models of structure, are discussed. Then, in Sec. III, we present and discuss the results of our analyses of the cross sections and analyzing powers. Conclusions we draw are given thereafter in Sec. IV.

II. NUCLEON-NUCLEUS SCATTERING AND NUCLEAR STRUCTURE

As indicated above, we have used a g -folding model for the optical potentials with which predictions of elastic scattering observables have been made. We give relevant details of

that model in the first of the subsections that follow. Those potentials then have been used to find the distorted waves in DWA calculations of inelastic scattering and some details of the scattering amplitudes that are evaluated are given in subsection II B. Only salient features are given since the theories have been elucidated quite fully in a review [1]. Then, in subsection II C, we describe the structure models used to provide the information required in those scattering theories, again in brief as they have been fully explained previously [8, 9].

A. g -folding model of optical potentials

With this model, a microscopic complex, nonlocal, and energy-dependent optical potential is obtained from folding an effective NN interaction with the OBDME, which for the moment we take to include the wave functions of the individual bound nucleons, determined from a nucleon-based model of the structure of the nuclear target state. While three- (and more)-body effects are not considered explicitly in this approach, many-nucleon correlations are part of the structure calculations and, inherently, in the scattering calculations through the medium dependence of the effective NN interactions used.

In coordinate space the g -folding optical potential can be written as [1]

$$U(\mathbf{r}_1, \mathbf{r}_2; E) = \delta(\mathbf{r}_1 - \mathbf{r}_2) \sum_n \zeta_n \int \varphi_n^*(\mathbf{s}) v_D(R_{1s}) \varphi_n(\mathbf{s}) d\mathbf{s} + \sum_n \zeta_n \varphi_n^*(\mathbf{r}_1) v_{Ex}(R_{12}) \varphi_n(\mathbf{r}_2), \quad (1)$$

where D and Ex denote the sets of elements of the NN effective interaction that define direct and exchange parts of the NA optical potential. In this form, ζ_n are the shell occupancies in the target state, though more generally they are the OBDME if there are non-Hartree contributions possible. $\varphi_n(\mathbf{r})$ are the single-nucleon bound-state wave functions.

The direct term in Eq. (1) is the well-known $g\rho$ form of the optical potential,

$$V_D(\mathbf{r}_1) = \delta(\mathbf{r}_1 - \mathbf{r}_2) \sum_n \zeta_n \int \varphi_n^*(\mathbf{s}) v_D(R_{1s}) \varphi_n(\mathbf{s}) d\mathbf{s} = \delta(\mathbf{r}_1 - \mathbf{r}_2) \int \rho(\mathbf{s}) v_D(R_{1s}) d\mathbf{s}. \quad (2)$$

It is local by definition. Nonlocality of the optical potential arises from the explicit exchange terms, neglect of which can lead to serious problems. Localization of these non-localities, even if one forms a phase equivalent interaction, is no panacea. Of course, to follow a better approach requires use of credible nucleon-based models of the target structure.

B. Proton inelastic scattering

Inelastic scattering calculations have been made using the DWA with the effective NN interaction taken in the folding to define the optical potential as the transition operator.

With \mathcal{A}_{01} being a two-nucleon state antisymmetrization operator, the transition amplitudes for nucleon inelastic scattering through a scattering angle θ and between states J_i, M_i and J_f, M_f in a nuclear target, have the form [1]

$$\begin{aligned} \mathcal{T} &= T_{J_f J_i}^{M_f M_i \nu' \nu}(\theta) \\ &= \left\langle \chi_{\nu'}^{(-)}(\mathbf{k}_o 0) \right| \left\langle \Psi_{J_f M_f}(1 \cdots A) \right| A g_{\text{eff}}(0, 1) \mathcal{A}_{01} \left\{ \left| \chi_{\nu}^{(+)}(\mathbf{k}_i 0) \right\rangle \left| \Psi_{J_i M_i}(1 \cdots A) \right\rangle \right\}. \end{aligned} \quad (3)$$

In this, distorted wave functions are denoted by $\chi_\nu^\pm(q)$ for an incoming/outgoing proton with spin projection ν , wave vector \mathbf{k} , and coordinate set "q". The A -nucleon nuclear structure wave functions are denoted by $\Psi_{JM}(1 \cdots A)$, and since all of pairwise interactions between the projectile and every target nucleon are taken to be the same, it is convenient to make cofactor expansions i.e.

$$|\Psi_{JM}(1, \cdots A)\rangle = \frac{1}{\sqrt{A}} \sum_{j,m} |\varphi_{jm}(1)\rangle a_{jm}(1) |\Psi_{JM}(1 \cdots A)\rangle. \quad (4)$$

Thus the transition amplitudes expand to the form

$$\begin{aligned} \mathcal{T} = & \sum_{j_1, j_2} \langle \Psi_{J_f M_f}(1 \cdots A) | a_{j_2 m_2}^\dagger(1) a_{j_1 m_1}(1) | \Psi_{J_i M_i}(1 \cdots A) \rangle \\ & \times \left\langle \chi_{\nu'}^{(-)}(\mathbf{k}_o 0) \left| \langle \varphi_{j_2 m_2}(1) | g_{\text{eff}}(0, 1) \mathcal{A}_{01} \left\{ |\chi_\nu^{(+)}(\mathbf{k}_i 0) \rangle |\varphi_{j_1 m_1}(1)\rangle \right\} \right. \right\rangle, \end{aligned} \quad (5)$$

where the many-body matrix elements of particle-hole operators are expressed by

$$\begin{aligned} \rho = & \langle \Psi_{J_f M_f}(1, \cdots A) | a_{j_2 m_2}^\dagger(1) a_{j_1 m_1}(1) | \Psi_{J_i M_i}(1 \cdots A) \rangle \\ = & \sum_{I(N)} (-1)^{(j_1 - m_1)} \langle j_1 j_2 m_1 - m_2 | I - N \rangle \langle \Psi_{J_f M_f} | [a_{j_2}^\dagger(1) \times a_{j_1}(1)]^{IN} | \Psi_{J_i M_i} \rangle \\ = & \sum_{I(N)} (-1)^{(j_1 - m_1)} \langle j_1 j_2 m_1 - m_2 | I - N \rangle \frac{1}{\sqrt{2J_f + 1}} \langle J_i I M_i N | J_f M_f \rangle S_{j_1 j_2 I}^{J_i \rightarrow J_f}, \end{aligned} \quad (6)$$

on using the Wigner-Eckart theorem. The OBDME in the above equation are the reduced matrix elements,

$$S_{j_1 j_2 I}^{J_i \rightarrow J_f} = \langle \Psi_{J_f} | [[a_{j_2}^\dagger(1) \times a_{j_1}(1)]^I] | \Psi_{J_i} \rangle, \quad (7)$$

and so carry the multi-nucleon aspects of nuclear structure tested in this theory. Then the transition amplitude can be written,

$$\begin{aligned} \mathcal{T} = & \sum_{j_1, j_2, m_1, m_2, I(N)} (-1)^{(j_1 - m_1)} \frac{1}{\sqrt{2J_f + 1}} \langle J_i I M_i N | J_f M_f \rangle \langle j_1 j_2 m_1 - m_2 | I - N \rangle S_{j_1 j_2 I}^{(J_i \rightarrow J_f)} \\ & \times \left\langle \chi_{\nu'}^{(-)}(\mathbf{k}_o 0) \left| \langle \varphi_{j_2 m_2}(1) | g_{\text{eff}}(0, 1) \mathcal{A}_{01} \left\{ |\chi_\nu^{(+)}(\mathbf{k}_i 0) \rangle |\varphi_{j_1 m_1}(1)\rangle \right\} \right. \right\rangle. \end{aligned} \quad (8)$$

As with the generation of the elastic scattering, and so also of the distorted wave functions for use in the DWA evaluations, antisymmetry of the projectile with the individual bound nucleons is treated exactly. The associated knock-out (exchange) amplitudes contribute importantly to the scattering cross section, both in magnitude and shape.

1. The effective NN interaction

A key element in both the g -folding and DWA prescriptions is the effective NN interaction, $g_{\text{eff}}(0, 1)$. This we require to be specified in coordinate space and in a form that can be used with the DWBA98 programs [13]. For that, these effective interactions can be constructed having central (C), tensor (S_{12}), and two-body spin-orbit ($L \cdot S$) components;

each of which has a form factor that is a sum of Yukawas of various ranges. Each of those Yukawas can have a complex strength which is dependent upon both the incident energy and the density of the nucleus. With $r = |\mathbf{r}_0 - \mathbf{r}_1|$ and energy ω ,

$$g_{eff}^{ST}(r, \omega) = \sum_i \langle \theta_i \rangle \sum_{j=1}^{n_i} S_j^{(i)}(\omega) \frac{e^{-\mu_j^{(i)} r}}{r}. \quad (9)$$

Here θ_i are the characteristic operators for central forces ($i = 1$), $\{1, (\sigma \cdot \sigma), (\tau \cdot \tau), (\sigma \cdot \sigma \tau \cdot \tau)\}$, for the tensor force ($i = 2$), $\{\mathbf{S}_{12}\}$, and the two-body spin-orbit force ($i = 3$), $\{\mathbf{L} \cdot \mathbf{S}\}$. $S_j^{(i)}(\omega)$ are complex, energy- and medium-dependent strengths, $\mu_j^{(i)}$ are the inverse ranges of the interaction, and j represents the set of the inverse ranges chosen. In principle, the number of strengths and inverse ranges (n_i) chosen can be as large as one likes, though for all operators and for non-relativistic energies, $n_i = 4$ seems to be sufficient for one to reproduce the on- and half-off-shell g -matrices within 32 NN S, T channels. We consider what those g -matrices are, and how the g_{eff} is mapped against them, next.

The nuclear g -matrices we take to be solutions of the Bethe-Brueckner-Goldstone (BBG) equations for infinite nuclear matter, i.e. of

$$g_{L,L'}^{JST}(p', p; k; k_f) = V_{L,L'}^{JST}(p', p) + \frac{2}{\pi} \sum_l \lim_{\varepsilon \rightarrow 0} \int_0^\infty V_{L,l}^{(JST)}(p', q) [\mathcal{H}_\varepsilon] g_{l,L'}^{(JST)}(q, p; k, k_f) q^2 dq. \quad (10)$$

The propagator term, \mathcal{H}_ε , is

$$\mathcal{H}(q, k, K, k_f) = \frac{\bar{Q}(q, K; k_f)}{\bar{E}(q, K; k_f) - \bar{E}(q, K; k_f) - i\varepsilon} \quad (11)$$

in which $\bar{Q}(q, K; k_f)$ is an angle average Pauli operator with an average center of mass momentum K and for Fermi momentum k_F . A range of Fermi momenta spanning free space to 1.5 central nuclear densities have been considered. The energies in the propagators of the BBG equations include an auxiliary potential U , and are defined by

$$\bar{E}(q, K; k_f) = \frac{\hbar^2}{m} (q^2 + K^2) + U(|\mathbf{q} + \mathbf{K}|) + U(|\mathbf{q} - \mathbf{K}|). \quad (12)$$

Full details of these quantities are found in Ref. [1].

The coordinate space effective NN interactions of Eq. (9) then have been defined by mapping double Bessel transforms of them to the on- and a range of half-off-shell values of those g -matrices with Fermi momenta set by the density of the nucleus at the central point between the pair. Details are given in Ref. [1].

C. Models of structure

From the specifics of the scattering potentials and amplitudes given above, two details need be provided by the model chosen to describe the structure of the target. Those details are the OBDME and the single-nucleon bound-state wave functions. For the nuclei considered, the models from which those properties have been determined are discussed in brief next. We consider 10 single-particle states in scattering calculations, each identified by the state number listed in Table I.

TABLE I: Nomenclature of single-particle orbits.

ID	nl_j	ID	nl_j	ID	nl_j
1	$0s_{\frac{1}{2}}$	4	$0d_{\frac{5}{2}}$	7	$0f_{\frac{7}{2}}$
2	$0p_{\frac{3}{2}}$	5	$0d_{\frac{3}{2}}$	8	$0f_{\frac{5}{2}}$
3	$0p_{\frac{1}{2}}$	6	$1s_{\frac{1}{2}}$	9	$1p_{\frac{3}{2}}$
				10	$1p_{\frac{1}{2}}$

1. No-core shell model for ^{12}C

A no-core shell model calculation has been made to define the spectrum of ^{12}C , the ground-state shell occupancies, and the OBDME for the excitation of the 2_1^+ , (4.43 MeV) state [7]. The code OXBASH [14] was used with augmented MK3W potentials and with a complete $(0 + 2)\hbar\omega$ basis to define the positive parity states in the spectrum to 20 MeV excitation. With the exception of the well known strongly deformed 0_2^+ state, all other states were found within a few hundred keV of their known excitations. In particular, the predicted excitation energy of the 2_1^+ state was 4.62 MeV.

The ground-state occupancies found from this shell model study are dominantly those of the $0s_{\frac{1}{2}}$ (1.964)-, $0p_{\frac{3}{2}}$ (3.054)-, and $0p_{\frac{1}{2}}$ (0.842)-shells (for both protons and neutrons); the remaining 0.14 nucleons being in the higher orbits. The OBDME for inelastic scattering are given in Table II. Using these OBDME in evaluations of the $B(E2; 2^+ \rightarrow 0^+(gs))$ with bare

TABLE II: The OBDME for excitation of the 2_1^+ state in ^{12}C .

j_2	j_1	$S_{j_1 j_2, 2}$	j_2	j_1	$S_{j_1 j_2, 2}$	j_2	j_1	$S_{j_1 j_2, 2}$
2	2	0.5609	7	2	-0.1391	10	8	-0.0004
3	2	-1.0706	8	2	0.0530	2	9	0.0093
2	3	0.7728	9	2	-0.0136	3	9	-0.0042
4	1	-0.1586	10	2	0.0270	7	9	-0.0011
5	1	0.1356	8	3	-0.0526	8	9	0.0007
1	4	-0.1586	9	3	0.0003	2	10	0.0055
4	4	0.0174	2	7	-0.0576	8	10	-0.0004
5	4	-0.006	7	7	-0.0038			
6	4	0.0026	8	7	0.0010			
1	5	-0.0949	9	7	-0.0008			
4	5	0.0042	2	8	-0.0398			
5	5	0.0087	3	8	-0.0071			
6	5	0.0012	7	8	-0.0020			
4	6	0.0013	8	8	-0.0007			
5	6	-0.0016	9	8	-0.0001			

charges gave a value of $6.26 e^2\text{-fm}^4$ when HO wave functions with oscillator length of 1.7 fm was used. This compares very favorably with the known value of $7.77e^2\text{-fm}^4$, especially when the Cohen and Kurath ($0\hbar\omega$ shell model) gives $3.26 e^2\text{-fm}^4$, on which, the no-core large

space model of Navratil, Vary, and Barrett [15] only slightly improves. By holding fast to an NN interaction defined for free space NN collisions in their model, and as they note in the article, they did not account sufficiently for multi-particle correlations in nuclear structure.

2. PHF and SHF plus shell models for ^{20}Ne , ^{24}Mg , ^{28}Si , and ^{40}Ca

Using the SHF model of structure, charge-density distributions and the associated nuclear radii have been calculated previously [9]. The resulting wave functions gave form factors in very good agreement with available data from electron scattering. Two forms of the Skyrme interaction were used, the so-called SkX_{csb} [8] and SkM^* [16] interactions. The SkX_{csb} Hamiltonian is based on the SkX Hamiltonian [17] with a charge-symmetry-breaking (CSB) interaction added to account for nuclear displacement energies [8]. The charge densities from all three calculations are very similar and so we only use those determined from the SkX_{csb} model (referred to hereafter as simply “SkX”). There are some small $\leq 5\%$ differences in the interior densities found with these models but they have little effect on scattering results; especially of the total reaction cross sections [18]. Generally, with this SHF method, good agreement between theory and experiment has been achieved in extensive comparisons of measured nuclear charge-density distributions with calculated values for p -shell, sd -shell, and pf -shell nuclei and some selected magic and semi-magic nuclei up to ^{208}Pb . With the pure SkX model, proton and neutron densities differ slightly. While such differences do not effect scattering results much, the small differences have been noted in determining a value for the neutron skin in ^{208}Pb [5].

The ground-state shell occupancies found from the SHF plus shell model studies [9] of the nuclei, ^{20}Ne to ^{40}Ca are listed in Table III.

TABLE III: Shell occupancies from the SHF plus shell model calculations of the listed nuclei

ID	^{20}Ne	^{24}Mg	^{28}Si	^{40}Ca
1	2.000	2.000	2.000	2.000
2	4.000	4.000	4.000	4.000
3	2.000	2.000	2.000	2.000
4	1.209	2.990	4.623	6.000
5	0.283	0.563	0.673	3.090
6	0.508	0.448	0.704	1.800
7	—	—	—	0.990
8	—	—	—	0.000
9	—	—	—	0.120
10	—	—	—	0.000

While much success has been had using the SHF densities and wave functions generated using the SkX model, the canonical wave functions may not have a desirable long range character. So we have also used Woods-Saxon (WS) single-nucleon bound-state wave functions to compare scattering results. For these nuclei, the SkX calculations only give ground-state properties while SM studies, that do provide transition OBDME [12], have not been made with a large enough basis. Consequently, we resorted to PHF evaluations to define the OB-

DME to be used in calculations of inelastic scattering to the 2_1^+ states. For completeness, these OBDME are listed in Table IV.

TABLE IV: OBDME for the transitions to the 2_1^+ states (values for which at least one entry $> \pm 0.02$). $j_2, (j_1)$ are a list of particle (hole) terms with identification as in Table III.

j_2	j_1	^{20}Ne	^{24}Mg	^{28}Si
4	4	0.592	0.8308	0.7088
5	4	-0.169	-0.5738	-0.6542
6	4	0.601	0.6818	0.6331
4	5	0.121	0.5954	0.6111
5	5	0.107	-0.0151	0.4549
6	5	0.193	0.1969	0.1481
4	6	0.752	0.5428	0.6782
5	6	-0.341	-0.2321	-0.2865
4	1	-0.190	-0.1641	-0.2475
5	1	0.128	0.1229	0.1541
1	4	-0.148	-0.2092	-0.2250
1	5	-0.081	-0.1027	-0.0950
7	2	-0.147	-0.2270	-0.2074
8	2	0.089	0.1054	0.1001
9	2	-0.058	-0.0368	-0.0393
10	2	0.049	0.0302	0.0287
8	3	0.180	-0.2169	-0.1864
9	3	-0.060	-0.0377	-0.0318
2	7	-0.131	-0.1762	-0.1659
9	7	-0.027	-0.0464	-0.0456
2	8	-0.067	-0.0819	-0.0802
3	8	-0.135	-0.1685	-0.1492
7	8	0.004	0.0046	-0.0044
9	8	-0.014	-0.0216	-0.0217
10	8	-0.018	-0.0368	-0.0346
2	9	-0.042	-0.0274	-0.0303
3	9	0.016	0.0283	0.0246
7	9	-0.035	-0.0602	-0.0565
8	9	0.018	0.0280	0.0270
9	9	-0.022	-0.0178	-0.0208
2	10	-0.036	-0.0226	-0.0221
8	10	-0.024	-0.0476	-0.0430
9	10	-0.016	-0.0147	-0.0148

III. RESULTS AND DISCUSSIONS

We analyze the differential cross sections and analyzing powers from elastic and inelastic (to 2_1^+ states) scattering off ^{12}C , ^{20}Ne , ^{24}Mg , ^{28}Si and ^{40}Ca . Analyses are made at non-relativistic energies for each case where data exist for proton scattering.

A. Elastic and inelastic scattering of protons from ^{12}C

In Fig. 1, the cross sections and analyzing powers for elastic scattering data [19, 20, 21, 22, 23, 24] of 35, 51.93, 120, 160, 200 and 250 MeV protons from ^{12}C are compared with the results found using the g -folding model. Traditionally one chooses either HO or WS

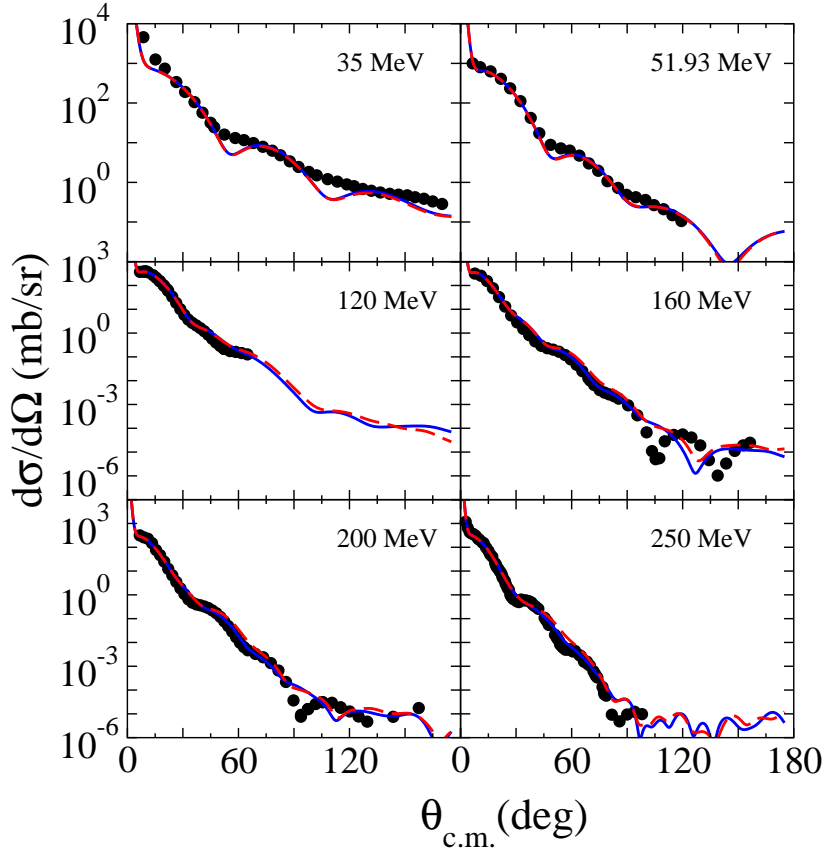


FIG. 1: (Color online) g -folding model predictions of cross sections for the elastic scattering of 35, 51.93, 120, 160, 200 and 250 MeV protons from ^{12}C compared with data [19, 20, 21, 22, 23, 24]. The predictions found by using HO wave functions are shown by the solid curves while those obtained with the WS single-particle wave functions are displayed by the dashed curves.

functions for the bound-state single-particle wave functions. The solid curves in this figure are the results obtained using the HO model of structure, while the dashed curves are those obtained when WS bound-state wave functions are used. As shown in Fig. 1, the predictions of cross sections are in quite good agreement with experimental data up to 170° scattering, in those cases where the data extend to this scattering angle. But the minima of 35 and

51.93 MeV calculated results are more sharply defined than seen in data. It is evident that back angle data are not well described by the predictions, but the cross section values are very small, usually much less than a mb/sr. Small variations in the details used in our calculations, as well as other reaction process effects not considered within the g -folding approach (if such have influence), will affect small cross-section values most obviously.

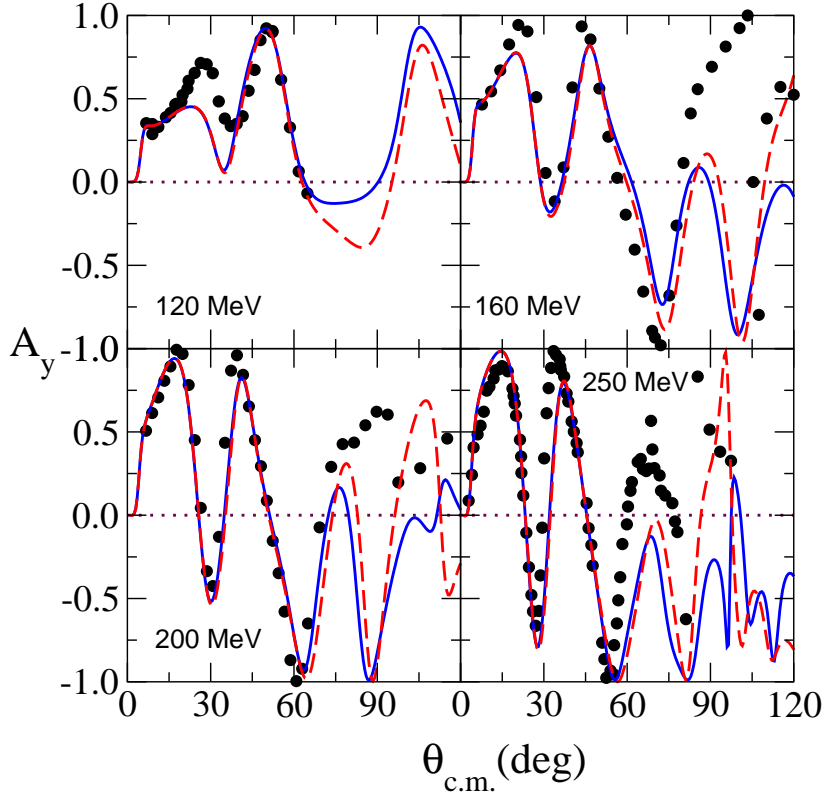


FIG. 2: (Color online) g -folding model predictions of analyzing powers for the elastic scattering of 120, 160, 200 and 250 MeV protons from ^{12}C compared with data [21, 22, 23, 24]. The notation is as used in Fig. 1.

In Fig. 2, we compare our calculated analyzing powers from proton elastic scattering on ^{12}C with the data that have been taken at 120, 160, 200 and 250 MeV [21, 22, 23, 24]. Clearly our predictions match observation quite well up to $\sim 70^\circ$ scattering and for all four energies. But there are noticeable discrepancies at large angles. HO and WS results are shown by the solid and dashed curves respectively, and they are almost indistinguishable over the range of scattering angles at which we find good representation of the data. Differences between the HO and WS results appear explicitly as the angle increases, though neither result makes a match to observation there. But one must remember that analyzing powers are normalized against the scattering cross section; data against measured values and theoretical ones against theoretical cross sections. Thus wherever theory does not give a sufficiently good representation of cross-section data, a match to analyzing power data can only be considered fortuitous. Equally a mismatch must not be taken necessarily as consequential.

The cross sections from inelastic scattering of 35, 51.93, 120, 160, 200 and 250 MeV protons exciting the 2^+ ; 4.44 MeV state in ^{12}C are displayed in Fig. 3. The results of our

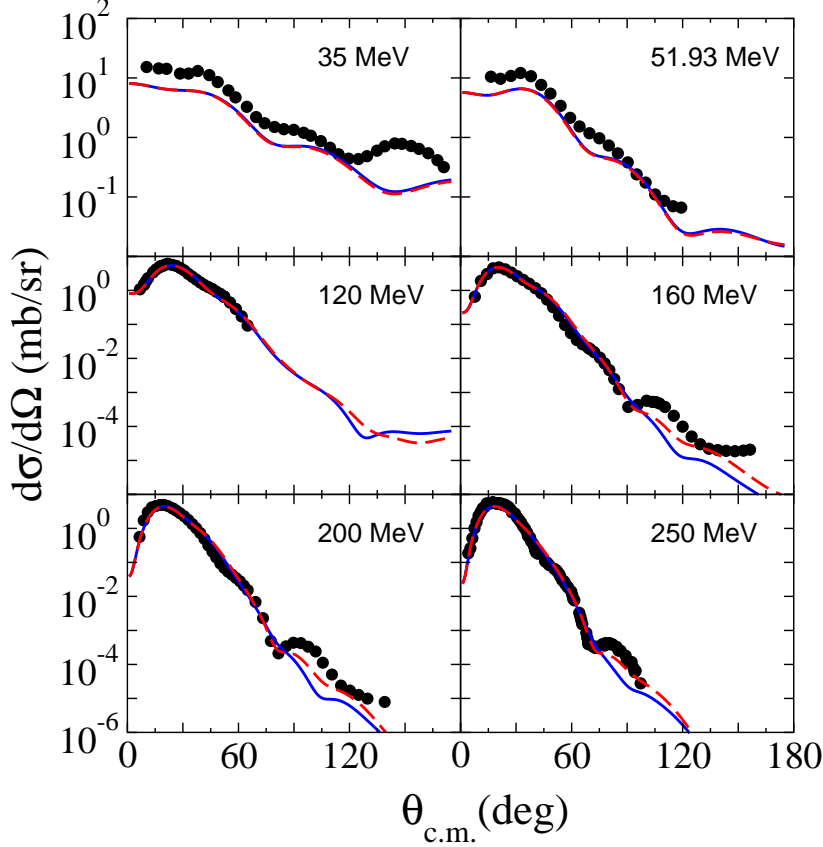


FIG. 3: (Color online) DWA cross sections for the inelastic scattering of 35, 51.93, 120, 160, 200 and 250 MeV protons from the excitation of the $2^+;4.44$ MeV state in ^{12}C compared with data [19, 20, 21, 25, 26]. The notation is as used in Fig. 1.

DWA calculations reproduce the shape and magnitude of these cross sections for all but the lowest energies, and to quite small magnitudes. Again the differences between results found using HO and WS single-nucleon bound-state wave functions are negligible until one has very small cross-section values. The HO and WS results are displayed by the solid and dashed curves respectively. These results bespeak of appropriate structure since the no-core shell model structure not only gave good results for the $B(E2)$ and electron scattering form factors [12], but now also for cross sections formed using the g -folding approach with the effective NN interactions for many different energies. There is clearly some other process required to explain the data at 35 and 51.93 MeV. Our g -folding results underestimate the data [19, 20, 21, 25, 26] by factors of 2.0 and 1.5 respectively. Further there is a noticeable difference in shape between our results and the data at large scattering angles for the 35 MeV case. Such is not caused by an inadequacy in the effective NN interaction. Recently, good results for these and even lower energies have been found in studies of ^6He scattering from hydrogen, both elastic and inelastic exciting the 2_1^+ state of ^6He . We believe that there are competing scattering processes that have been ignored; and processes that relate to this target and for these energies. Virtual excitation of giant resonances seems a most likely cause. Past studies of inelastic scattering of protons from ^{12}C have indicated that, at 35 MeV specifically, contributions from virtual excitation of isoscalar $E2$ and $E3$

resonances can contribute noticeably [27]. They do so as specific second order processes, first by enhancing direct scattering amplitudes (in which the incoming proton is also the emergent one) and by exchange amplitude contributions in which the incident proton is trapped with the giant resonance formed subsequently decaying by emitting the detected proton. That exchange process leads to cross-section contributions that are symmetric about 90° and of about a mb/sr in size [27]. The correction at large scattering angles needed in the 35 MeV result is characteristic of the corrections just such an exchange process would give [27], while the enhancements needed for both the 35 and 52 MeV results are consistent also with contributions from the direct effect of the second-order process involving giant resonances.

The DWA results for the analyzing power from 120, 160, 200 and 250 MeV protons exciting the 2^+ ; 4.44 MeV state in ^{12}C are compared with the data [21, 25, 26] in Fig. 4. The results found using HO and WS wave functions again are displayed by the solid and

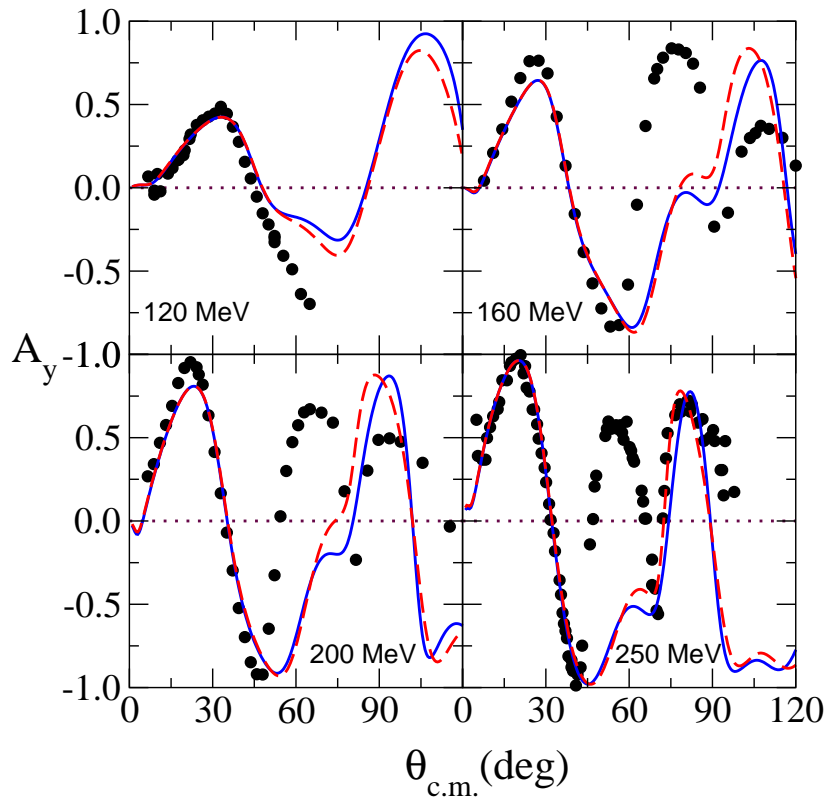


FIG. 4: (Color online) Analyzing powers for the inelastic scattering of 120, 160, 200 and 250 MeV protons from the excitation of the 2^+ ; 4.44 MeV state in ^{12}C compared with data [21, 25, 26].

dashed curves respectively. Those results have similar structures and are in good agreement with the data up to $\sim 45^\circ$. At larger scattering angles there are noticeable discrepancies between calculated results and the data. For these four energies, by 45° the cross sections are quite small (≤ 1 mb/sr) and so sensitive observables such as the analyzing power, as they are normalized against cross sections, can then show large effects caused by minor problems in detail.

B. Elastic and inelastic scattering of protons from ^{20}Ne

Our g -folding model predictions of the cross sections for the elastic scattering of 35.2 and 135.4 MeV protons from ^{20}Ne are compared with data in Fig. 5. Single-particle bound-state

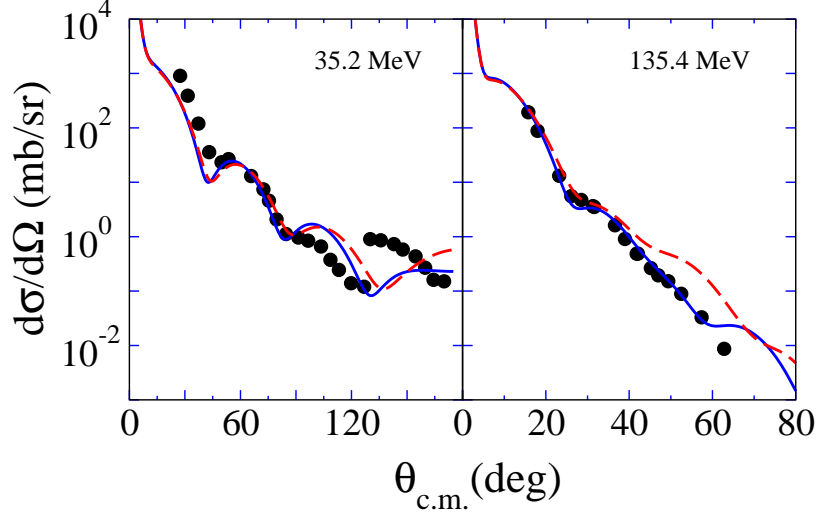


FIG. 5: (Color online) g -folding model predictions of cross sections for the elastic scattering of 35.2 and 135.4 MeV protons from ^{20}Ne compared with data [28, 29].

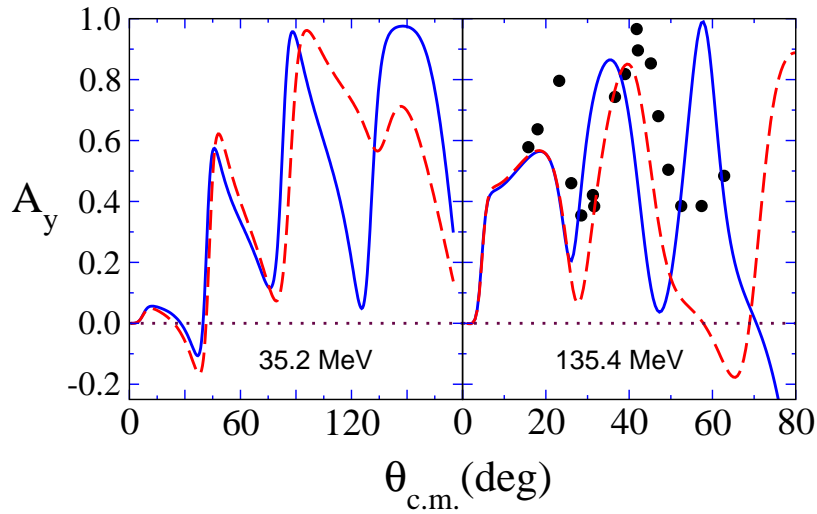


FIG. 6: (Color online) g -folding model predictions of analyzing powers for the elastic scattering of 35.2 and 135.4 MeV protons from ^{20}Ne compared with data [29].

wave functions were assumed to be either a WS set or those generated with the SHF method (with the SkX interaction). The solid curves display results obtained using the SHF wave functions, while dashed curves show those found with the WS wave functions. The 135.4 MeV cross-section data [29] are well reproduced by our calculations, especially when the SHF bound states are used. However, that degree of matching may be only fortuitous. The

cross section found with 35.2 MeV protons scattering from ^{20}Ne is reasonable to $\sim 90^\circ$, by which time the cross-section magnitude is 1 mb/sr, and the mismatch for larger scattering angles is reminiscent of an effect of virtual excitation of a giant resonance.

The elastic scattering analyzing power data [29] and g -folding model predictions are displayed in Fig. 6. The notation is the same as used in Fig. 5. There are no available data at 35.2 MeV and we display those results only to note what differences there are between use of WS and SHF single-nucleon bound-state wave functions. To $\sim 90^\circ$ scattering where both sets of wave functions give good cross-section results, there is practically no difference in the analyzing powers found. They do differ somewhat at larger scattering angles but then the actual cross sections are small and differ from both theoretical predictions. In the case of 135.4 MeV scattering, there are noticeable differences between predictions and data. Nevertheless the g -folding model results do show the data trend.

Differential cross sections from the inelastic scattering of protons to the 2^+ (1.633 MeV) state in ^{20}Ne found from DWA calculations are displayed in Fig. 7. No data have been taken at 35.2 MeV incident energy and the predictions made using SHF (solid curve) and WS (dashed curve) have been made simply to show that there are but minor effects due to the precise nature of the wave functions used. In the case of 135.4 MeV, DWA results under-

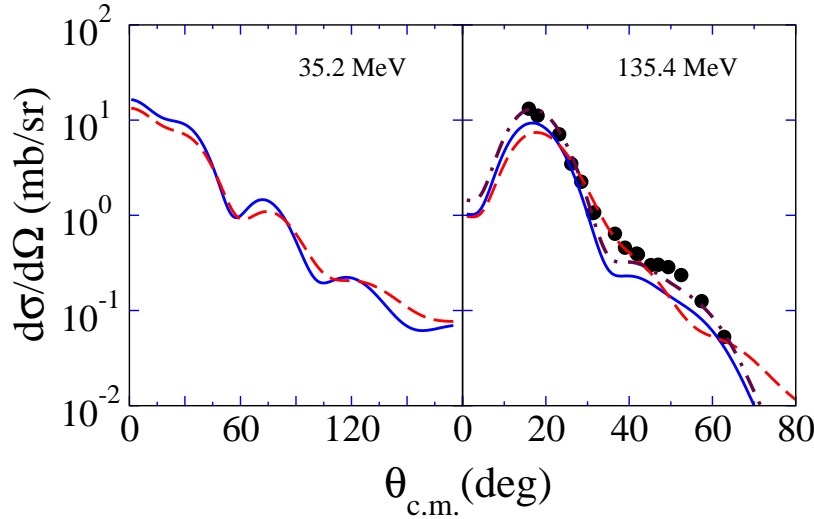


FIG. 7: (Color online) DWA cross sections for the inelastic scattering of 35.2 and 135.4 MeV protons from the excitation of the $2^+; 1.633$ MeV state in ^{20}Ne compared with data [29].

predict data [29]. If the SHF result is enhanced by 40%, a very good fit is found to that data. The dot-dash curve is the SHF cross section multiplied by a factor of 1.4. This enhancement, taken as a problem of theory, then can only be an effect of missing configuration mixing in the (PHF) structure model.

The analyzing powers from excitation of the 2^+ state is displayed in Fig. 8 where, again, the solid and dashed curves depict the SHF and WS results respectively. As with the cross sections, the results for the scattering of 35.2 MeV protons are very similar, while there are more differences between them seen in the 135.4 MeV results. As with the cross sections, agreement between the SHF result and the 135.4 MeV data [29] for scattering to the 2^+ state is quite good, while the WS result only follows the trend of data.

In the elastic and inelastic scattering analyzing powers from protons on ^{20}Ne , the WS results universally are shifted toward higher momentum transfer values when compared with

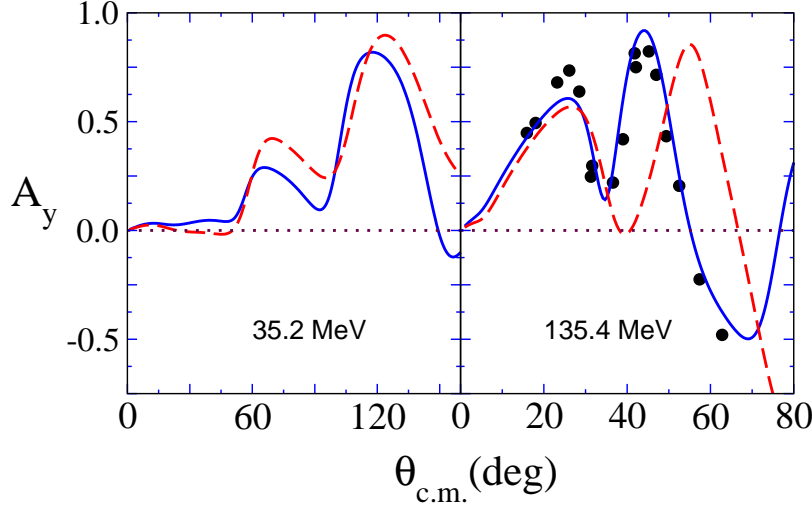


FIG. 8: (Color online) Analyzing powers for the inelastic scattering of 35.2 and 135.4 MeV protons from the excitation of the $2^+; 1.633$ MeV state in ^{20}Ne compared with data [29].

the SHF results. This is the prime feature that distinguishes the choice taken for single-particle wave functions.

C. Elastic and inelastic scattering of protons from ^{24}Mg

In Fig. 9, differential cross sections for the elastic scattering of protons from ^{24}Mg with energies of 34.9, 51.93, 134.7, and 250 MeV are shown. The results of calculations made using SHF wave functions are depicted by the solid curves, while those found from using WS wave functions are shown by the dashed curves. SHF predictions of the elastic cross sections made with the g -folding model agree very well with the data [20, 26, 30, 31] except for the overly sharp defined minima they give with the lower energies. For the two larger energies, these SHF results give better fits to the data than do those found using the WS functions, noticeably at large scattering angles.

Analyzing powers for proton elastic scattering from ^{24}Mg have been measured [26, 31] for incident energies of 134.7 and 250 MeV. That data are compared with our g -folding model results in Fig. 10. Again the solid and dashed curves depict results found using SHF and WS wave functions respectively. There are quite noticeable differences between these results. In these cases, the WS functions give the best representation of the data. As with the ^{20}Ne results, the WS results are shifted to higher momentum transfer values compared with those of SHF results.

DWA calculated cross sections for 35, 51.93, 185 and 250 MeV proton inelastic scattering to the 2_1^+ state at 1.37 MeV excitation in ^{24}Mg are compared with data [19, 20, 26, 32] in Fig. 11. The results that have been obtained using SkX model wave functions are displayed by the solid curves. The dashed curves portray those found by using the WS set of wave functions. The third result in each panel depicted by the dot-dashed curve is the SkX model cross section but enhanced by scale factors of 1.6, 2.5, 1.77 and 1.54 for the 35, 51.93, 185 and 250 MeV cases respectively. These results compare very well with the data.

Analyzing power data for inelastic scattering to the 2_1^+ state in ^{24}Mg have been taken with

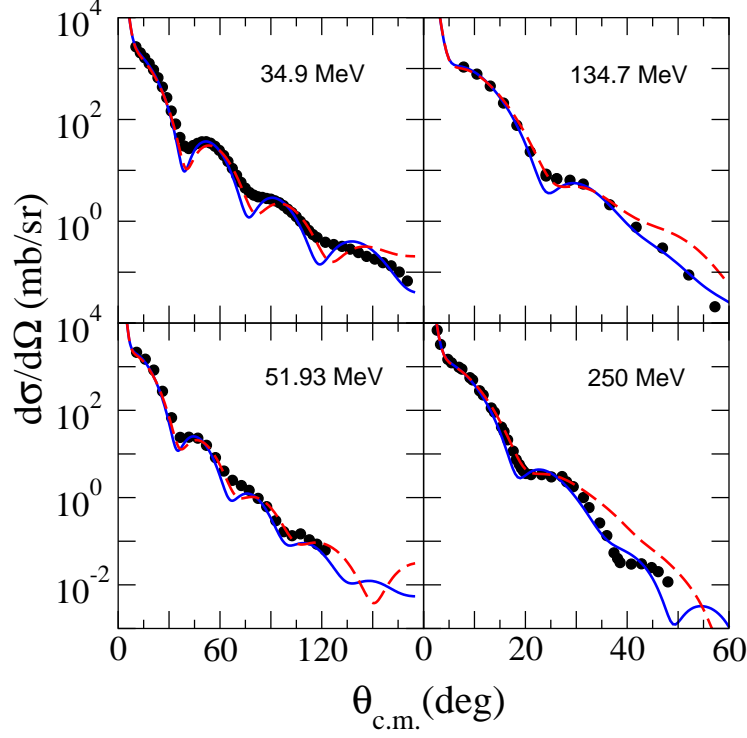


FIG. 9: (Color online) g -folding model predictions of cross sections for the elastic scattering of 34.9, 51.93, 134.7 and 250 MeV protons from ^{24}Mg compared with data [20, 26, 30, 31].

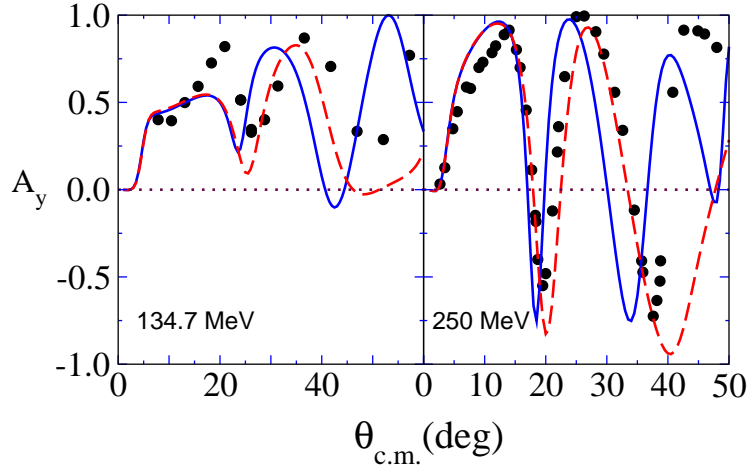


FIG. 10: (Color online) g -folding model predictions of analyzing powers for the elastic scattering of 134.7 and 250 MeV protons from ^{24}Mg compared with data [26, 31].

250 MeV protons [26]. We compare that data with the results of our calculations that were made using the SHF and WS sets of single-particle bound-state wave functions (notation as with Fig. 11) on the right of Fig. 12. The result obtained using the SkX model is in quite good agreement with the data; distinctly better than the result found with the WS functions. As with other results, the analyzing power predicted using the WS functions is shifted to larger angular momentum transfer in comparison with the SkX model one. That

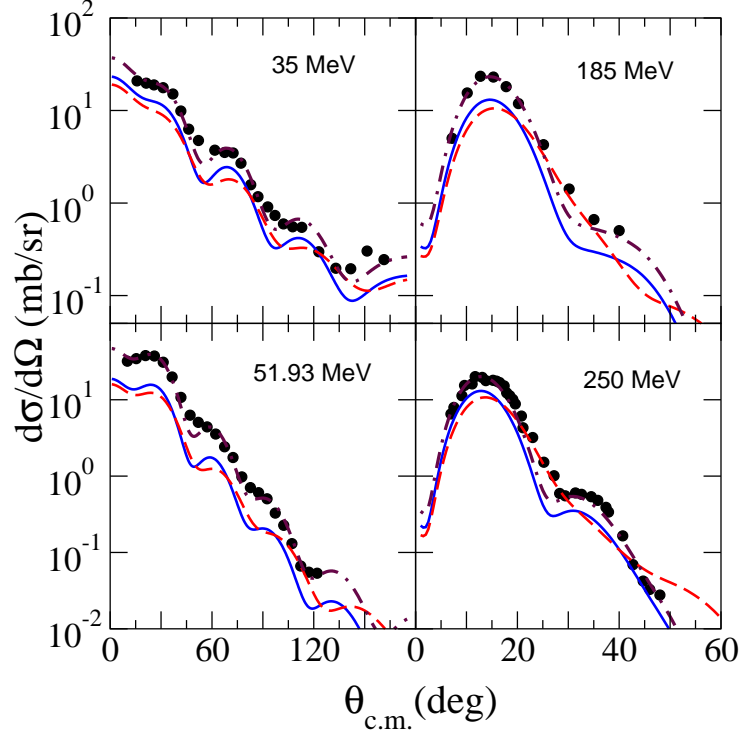


FIG. 11: (Color online) DWA cross sections for the inelastic scattering of 35, 51.93, 185 and 250 MeV protons from the excitation of the $2^+;1.37$ MeV state in ^{24}Mg compared with data [19, 20, 26, 32].

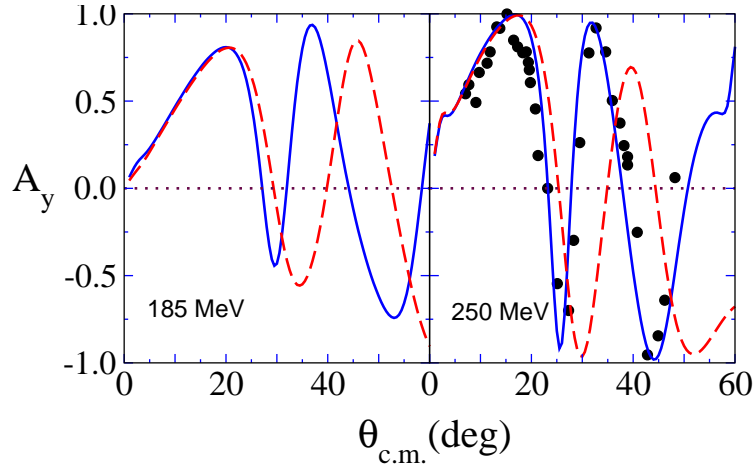


FIG. 12: (Color online) Analyzing powers for the inelastic scattering of 185 and 250 MeV protons from the excitation of the $2^+;1.37$ MeV state in ^{24}Mg compared with data [26].

distinction is also seen with the predictions shown in Fig. 12 for an energy of 185 MeV.

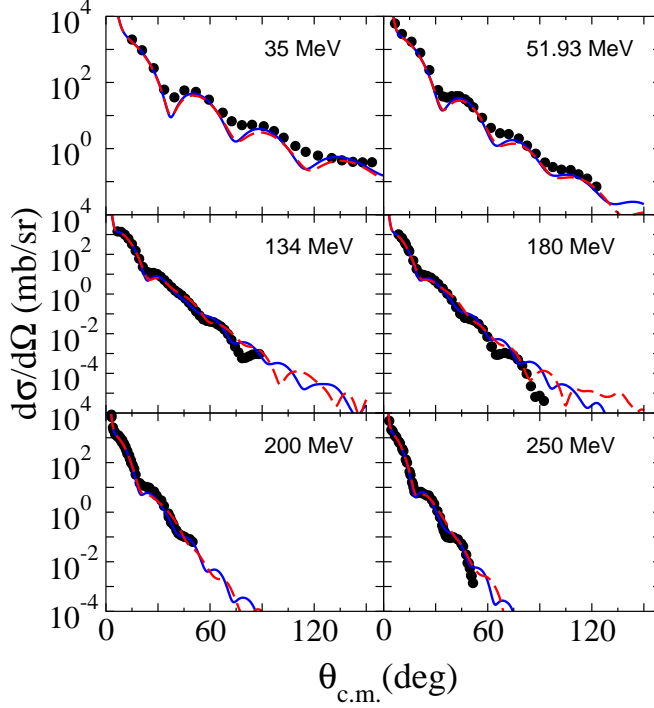


FIG. 13: (Color online) g -folding model predictions of cross sections for the elastic scattering of 35, 51.93, 134, 180, 200 and 250 MeV protons from ^{28}Si compared with data [19, 20, 26, 33].

D. Elastic and inelastic scattering of protons from ^{28}Si

The differential cross sections for 35, 51.93, 134, 180, 200 and 250 MeV protons elastically scattered from ^{28}Si are shown in Fig. 13. Therein data [19, 20, 26, 33] are compared with the results of calculations made using the SHF and WS sets of single-nucleon bound-state wave functions for this nucleus. The SHF and WS results are displayed by the solid and dashed curves, respectively. At 35 and 51.93 MeV, the minima of the g -folding results are more pronounced than as seen in the data. The magnitudes of the cross-section predictions also are slightly smaller than what is observed. There are no such problems with the comparisons of calculated cross sections and data for the higher energies, though, and as found with other targets, data and predictions do not match well at large scattering angles. As with other targets too, such discrepancies occur when the cross-section values are smaller than a few tenths of a mb/sr at most.

In Fig. 14, we present the results of the g -folding model calculations of analyzing powers from proton elastic scattering from ^{28}Si at four incident energies at which data has been taken [26, 33]. The notation used is that as in Fig. 13. The results for 134 MeV proton scattering do not match the data well though the general trend of the data is seen in the results, whether WS or SkX model structures are considered. At the higher energies, the SHF model results do match data quite well at least to scattering angles for which the cross sections are > 1 mb/sr; though there is a mismatch at forward scattering angles with the 250 MeV data. The main effect of the choice of single-nucleon bound-state wave functions, as seen previously, is again evident with the structure in the WS results spread to larger values of momentum transfer than found using the SkX model functions.

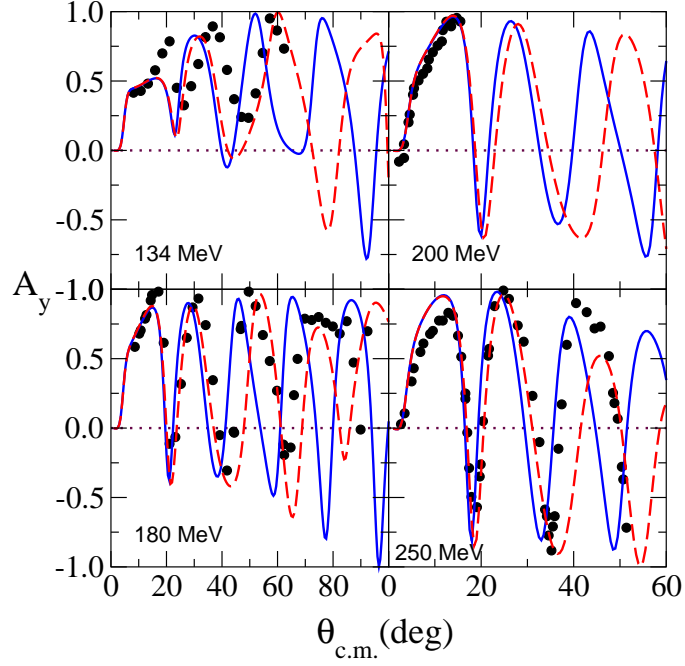


FIG. 14: (Color online) g -folding model predictions of analyzing powers for the elastic scattering of 134, 180, 200 and 250 MeV protons from ^{28}Si compared with data [26, 33].

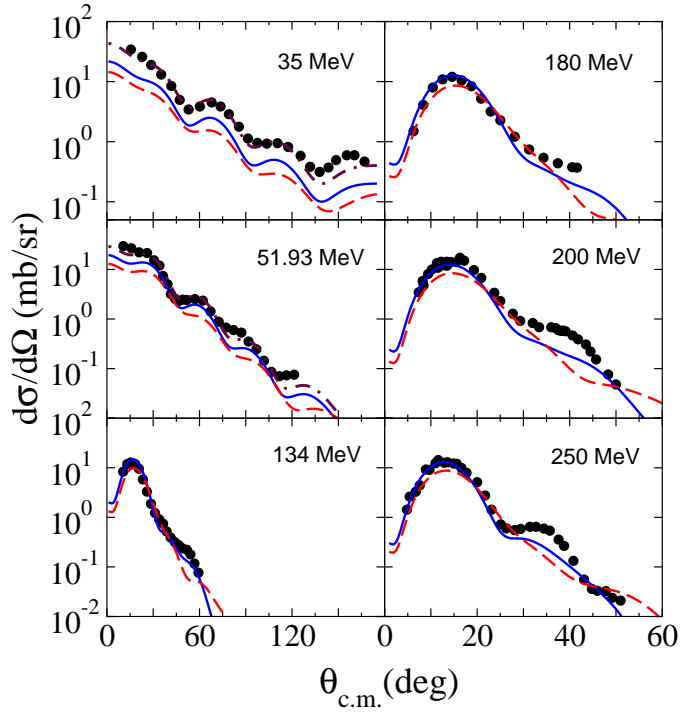


FIG. 15: (Color online) DWA cross sections for the inelastic scattering of 35, 51.93, 134, 180, 200 and 250 MeV protons from the excitation of the $2^+; 1.78$ MeV state in ^{28}Si compared with data [19, 20, 26, 34].

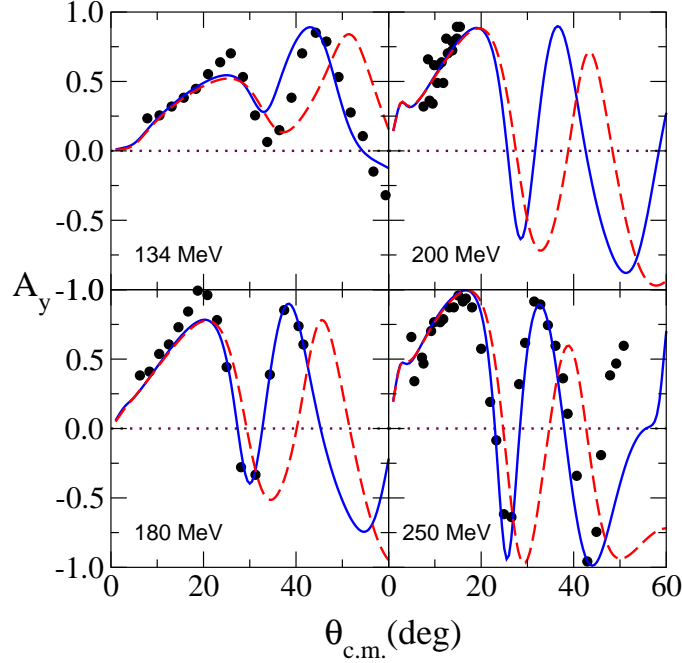


FIG. 16: (Color online) Analyzing powers for the inelastic scattering of 134, 180, 200 and 250 MeV protons from the excitation of the $2^+; 1.78$ MeV state in ^{28}Si compared with data [26, 34].

The cross sections resulting from DWA calculations of proton inelastic scattering to the $2^+(1.78 \text{ MeV})$ state in ^{28}Si are compared with data [19, 20, 26, 34] in Fig. 15. Cross sections for six incident energies are shown with the solid and dashed curves again portraying results obtained by using, respectively, the SHF and WS sets of single-nucleon bound-state wave functions in the calculations. Both theoretical predictions lie below the data for the 35 and 51.93 MeV cases. However, quite good agreement with the measured values is found when the SHF results are multiplied by factors of 2.0 and 1.5, respectively. Those enhanced results are depicted by the dot-dashed curves in the figure. At the higher energies, both model calculations match well the forward peak in the data and for which the data magnitude exceeds $\sim 1 \text{ mb/sr}$.

The analyzing power from inelastic proton scattering on ^{28}Si and leading to the $2^+(1.78 \text{ MeV})$ state has been measured at four energies. That data [26, 34] are compared with the results of our DWA calculations in Fig. 16. The notation is that as used in Fig. 15. The energies are 134, 180, 200, and 250 MeV, for which the predicted cross sections (shown in Fig. 15) match data quite well. Concomitantly, the SkX model results in particular match the measured analyzing powers very well. However, the distinctive feature in the analyzing power caused by the choice of single-particle bound-state wave functions, is again evident. Clearly the results found using the SkX set match the analyzing power data but those found using the WS set do not.

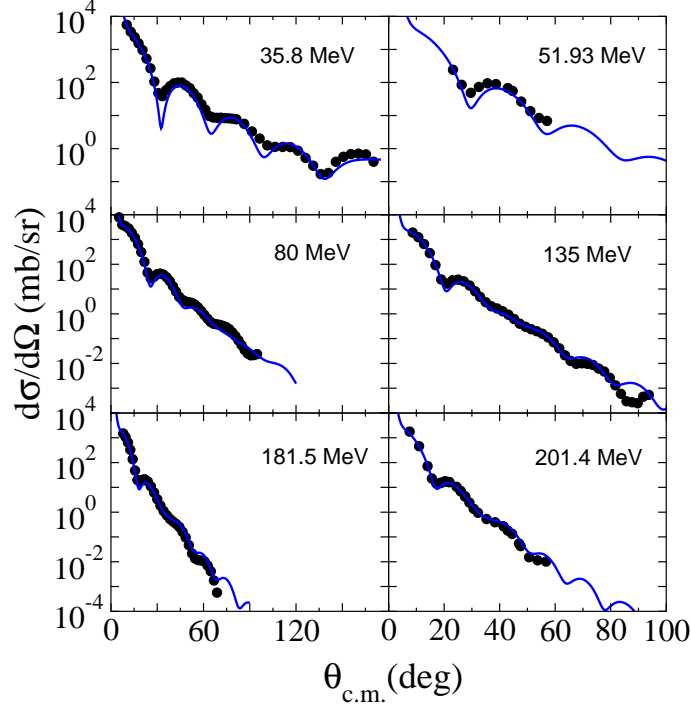


FIG. 17: (Color online) Differential elastic cross section predictions of 35.8, 51.93, 80, 135, 181.5 and 201.4 MeV protons scattering from ^{40}Ca compared with data [20, 35, 36, 37].

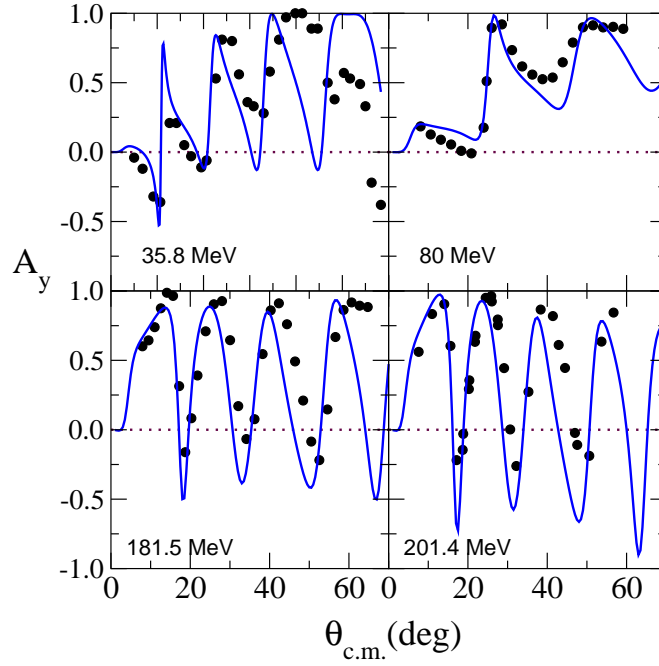


FIG. 18: (Color online) Analyzing powers predictions of 35.8, 80, 181.5 and 201.4 MeV protons elastically scattered from ^{40}Ca compared with data [31, 35, 37].

E. Elastic scattering of protons from ^{40}Ca

The results of our calculations, made using the SHF structure in the g -folding approach, of the elastic scattering of 35.8, 51.93, 80, 135, 181.5, and 201.4 MeV protons from ^{40}Ca are displayed by the solid curves in Fig. 17 and compared with differential cross-section data [20, 35, 36, 37]. At all energies, there is quite good agreement between the predictions and data though there are more pronounced minima seen theoretically in the cross sections for 35.8 and 51.93 MeV protons. For the energies between 80 and 201.4 MeV, our predictions track the data very well even to a magnitude of 0.01 mb/sr. The quality of these predictions are reflected in the match between the associated predictions and the data [31, 35, 37] for the analyzing powers. As is evident in Fig. 18, our g -folding model results reproduce the observations on the analyzing powers quite well. Notably, the structure falls at the correct momentum transfer values, the relative magnitudes of the oscillations are found correctly, the angle incline trend of the data at 35.8 and 80 MeV is reproduced, and the unusual shape feature of the data, once thought to be a relativistic effect, is found.

IV. CONCLUSIONS

Proton scattering data for non-relativistic energies (between 35 and 250 MeV) from ^{12}C , ^{20}Ne , ^{24}Mg , ^{28}Si and ^{40}Ca , have been analyzed to probe the character of the structure assumed for those targets. Differential cross sections and analyzing power data from both elastic scattering, and, for all but ^{40}Ca , inelastic scattering to the 2_1^+ states, have been studied. The elastic scattering data analyses have been made using a g -folding model for the optical potentials in which a complex, medium and energy dependent, effective NN interaction has been folded with the full one-body density matrices of each target. Three and higher-body interactions are assumed not to contribute significantly (in so far as magnitudes of cross sections are concerned at least). However, we maintained the Pauli principle in this approach, and the nonlocal terms in the optical potentials arising from ensuring that the Pauli principle is not violated, have very significant effects.

From those optical potential calculations, the proton-nucleus relative motion wave functions also have been found and used as the distorted waves within DWA evaluations of inelastic scattering observables. The effective NN interaction used in the g -folding to form the optical potentials then has been used as the transition operator effecting the inelastic scattering events. In the DWA approach we have used, the one body (transition) density matrices for the inelastic scattering are required as weightings on the single-particle states involved. Those single-particle states we take to be the same ones that we use in the g -folding.

With the methods and effective NN interactions proven credible from many past uses, when a structure has been chosen (OBDME, single-nucleon bound-state wave functions), then just one run of the relevant code (DWBA98) gives predictions of observables. Comparison of those with data then allows a critique of the assumed structure.

We have chosen a set of nuclei for which shell and Skyrme-Hartree-Fock models of structure have been used with some success to define their ground-state structures. With ^{12}C in particular, the no-core shell model with a complete $(0 + 2)\hbar\omega$ basis not only gave a good description of the positive parity spectrum, but also of the electromagnetic properties and electron scattering form factors. The Skyrme-Hartree-Fock studies when constrained against shell-model occupancies gave very good electron form factors for the sd -shell nuclei that we

consider. While the shell model also provided the structure details for excitation of the 2_1^+ state in ^{12}C , we resorted to using projected Hartree-Fock models to specify the OBDME for the excitations of the 2_1^+ states in ^{20}Ne , ^{24}Mg , and ^{28}Si , since no other model we know of yet can give estimates of those items in the size of basis we wished to consider. The single-particle bound-state wave functions were chosen to be either oscillator or Woods-Saxon in form for the evaluations with ^{12}C as target, and of either Woods-Saxon form or the canonical set used in each SHF evaluation with the other targets.

With the complete $(0 + 2)\hbar\omega$ space no-core shell model structure for ^{12}C , our g -folding model evaluations of elastic scattering cross sections and analyzing powers for protons with incident energies 35, 51.93, 120, 160, 200, and 250 MeV all match data very well. The distinctions between using oscillator or Woods-Saxon bound-state wave functions were slight. With the lowest two energies, there were more severe minima in the theoretical predictions than in the relevant data, but overall the results matched data well, especially for scattering angles where the data magnitude was greater than a few tenths of a mb/sr. The inelastic scattering results did not give as good a match to that cross-section data, but, with the exception of the results at 35 and 51.93 MeV, the predictions matched the dominant forward angle peaks in shape and magnitude. Only when data were small in magnitude, as they are at larger scattering angles, are discrepancies with predictions noted. Such is emphasized in the comparisons between predictions and data for the analyzing powers (data taken only at 120, 160, 200, and 250 MeV).

It is important that the correct transition strength is found from our calculations. This correlates with the close matching of the evaluated $B(E2)$ value from the chosen spectroscopy to the observed γ -decay and to the very good results found on using the same structure in evaluating electron scattering form factors. The under-prediction of the inelastic scattering cross sections at 35 MeV and, to a lesser extent, at 51.93 MeV then signals an effect of a process additional to the reaction mechanism we have assumed. The back angle bump in the 35 MeV inelastic scattering cross-section data indicates that the missing elements are due to virtual excitation of isoscalar $E2$ and/or $E3$ giant resonances.

There is little data available for ^{20}Ne , and with that our results give some ambivalence for interpretation. At 35.2 MeV only an average match is made to (elastic scattering) cross-section data that exceed 1 mb/sr. Perhaps there is an indication of virtual excitation of a giant resonance, but data of more precision and at other energies are needed to confirm such. The 135.4 MeV (elastic) cross-section data are very well described by the result from the g -folding model in which the SHF wave functions were used. But the analyzing power found from that calculation does not match the observed values. Inelastic scattering data, both cross section and analyzing power, have been measured with ^{20}Ne but only at 135.4 MeV. With these data however, using the DWA with OBDME from a PHF model (with SkX model single-particle wave functions) gave very good results when compared with the shapes of both cross-section and analyzing power data. Using WS wave functions did not give as good values. However, the bare prediction for the cross section had to be enhanced by 40% to meet the data. Interpreting that as evidence for more correlations (as a core polarization) equates to needing a polarization charge of just $0.1e$.

The elastic scattering cross sections from ^{24}Mg also are very well reproduced by predictions made using the g -folding model and the SHF set of wave functions. The results are preferable to those found using the WS functions but the discriminations are only by comparison of high momentum, small value, parts of the cross sections. The 34.9 MeV results have sharper structure than in the data. The elastic scattering analyzing powers, taken at

134.7 and 250 MeV, match the data only reasonably, and that at scattering angles for which the cross sections are larger than a mb/sr.

Using the PHF set of OBDME with the SHF single-particle wave functions in DWA calculations, underestimate the cross sections from proton inelastic scattering to the 2_1^+ state in ^{24}Mg . That is so at all four energies considered. The 51.93 MeV result is slightly exceptional to those at the other energies requiring an enhancement of 2.5 rather than the (average one of) 1.6. Treating this average enhancement as a core polarization requirement to the PHF structure assumed, equates to an effective charge of $0.13e$. Analyzing power data exist only for 250 MeV and the DWA result found using the SHF wave functions match that data well to 40° by which scattering angle, the cross section is but a tenth of a mb/sr.

Much the same as with ^{24}Mg is noted in regard to comparison of our g -folding model predictions of the elastic scattering observables from ^{28}Si . The sharper variation of predicted cross sections compared with the 35 and 51.93 MeV data is most obvious. However, the (elastic) analyzing power data from ^{28}Si are better replicated by our predictions than was the case with ^{24}Mg ; though the results at 135 MeV have larger discrepancy than is pleasing. Using the PHF model OBDME for the excitation of the 2_1^+ state in ^{28}Si with the SHF wave functions in DWA evaluations gave very good cross-section shapes in comparison with data taken at energies of 35, 51.93, 134, 180, 200, and 250 MeV. At least that was so for data that exceeded ~ 1 mb/sr. The match to the magnitudes also was good save that the results at 35 and 51.93 MeV required enhancing (by a factor of 2 and 1.5 respectively). Given that no such enhancement was required to match data at the higher energies, and given that the effective interactions at all energies considered seem well established, it is tempting to view these 35 and 51.93 MeV results as suggestive of virtual excitation of giant resonance effects. Much more data are needed to make such more than speculation however.

Finally we considered the data from proton elastic scattering from ^{40}Ca . Over the range of energies studied, the data, especially the analyzing powers, show considerable variation. That variation is remarkably well defined by our predictions made using the SHF structure model giving much credibility to the effective NN force we have used.

These results serve as indicators to what is needed when analyzing data from RIB scattering from hydrogen (and in fact from any other light mass target) are taken at energies within the range of giant resonance excitation of the exotic ion, if such should exist. Furthermore, our results have shown how important it is, not only to use a credible theory of scattering but also one of structure. Reaction processes not considered, effects due to inherent violation of the Pauli principle in scattering, and inadequate structure, possibly even equating to just a need for the ubiquitous $0.5e$ polarization charge, may be masked by judicious choice of parameter values and arbitrary scale factors. The more such have to be used, the less physics the analysis can yield.

Acknowledgments

This research was supported by a 2007 research grant of the Cheju National University and by the National Research Foundation of South Africa.

-
- [1] K. Amos, P. J. Dortmans, H. V. von Geramb, S. Karataglidis, and J. Raynal, *Adv. in Nucl. Phys.* **25**, 275 (2000), (and references contained therein).
 - [2] L. Canton, G. Pisent, J. P. Svenne, D. van der Knijff, K. Amos, and S. Karataglidis, *Phys. Rev. Lett.* **94**, 122503 (2005).
 - [3] K. Amos, S. Karataglidis, D. van der Knijff, L. Canton, G. Pisent, and J. P. Svenne, *Phys. Rev. C* **72**, 064604 (2005).
 - [4] S. V. Stepantsov et al., *Phys. Letts.* **B542**, 35 (2002).
 - [5] S. Karataglidis, K. Amos, B. A. Brown, and P. K. Deb, *Phys. Rev. C* **65**, 044306 (2002).
 - [6] B. A. Brown, *Phys. Rev. Letts.* **85**, 5296 (2000).
 - [7] S. Karataglidis, P. J. Dortmans, K. Amos, and R. de Swiniarski, *Phys. Rev. C* **53**, 838 (1995).
 - [8] B. A. Brown, W. A. Richter, and R. Lindsay, *Phys. Lett.* **B483**, 49 (2000).
 - [9] W. A. Richter and B. A. Brown, *Phys. Rev. C* **67**, 034317 (2003).
 - [10] P. Nesci and K. Amos, *Nucl. Phys.* **A284**, 239 (1977).
 - [11] P. Nesci, K. Amos, and I. Morrison, *J. Phys.* **G5**, 387 (1979).
 - [12] S. Karataglidis, P. Halse, and K. Amos, *Phys. Rev. C* **51**, 2494 (1995).
 - [13] J. Raynal (1998), computer program DWBA98, NEA 1209/05.
 - [14] B. A. Brown, A. Etchegoyen, and W. D. M. Rae (1986), oXBASH-MSU (the Oxford Buenos-Aries Michigan State University shell model code) MSU-NSCL Report Number 524.
 - [15] P. Navrátil, J. P. Vary, and B. R. Barrett, *Phys. Rev. C* **62**, 054311 (2000).
 - [16] J. Bartel, P. Quentin, M. Brack, C. Guet, and M. B. Hakansson, *Nucl. Phys.* **A386**, 79 (1982).
 - [17] B. A. Brown, *Phys. Rev. C* **58**, 220 (1998).
 - [18] K. Amos, W. A. Richter, S. Karataglidis, and B. A. Brown, *Phys. Rev. Lett.* **96**, 032503 (2006).
 - [19] M. Pignanelli, S. Micheletti, R. D. Leo, S. Brandenburg, and M. N. Harakeh, *Phys. Rev. C* **33**, 40 (1986).
 - [20] H. Ohnuma, J. Kasagi, and F. Kakimoto, *J. Phys. Soc. Japan* **48**, 1812 (1980).
 - [21] J. Comfort, G. L. Moake, C. C. Foster, P. Schwandt, C. D. Goodman, J. Rappaport, and W. G. Love, *Phys. Rev. C* **24**, 1834 (1981).
 - [22] H. O. Meyer, P. Schwandt, W. W. Jacobs, and J. R. Hall, *Phys. Rev. C* **27**, 459 (1983).
 - [23] H. O. Meyer, P. Schwandt, G. L. Moake, and P. P. Singh, *Phys. Rev. C* **23**, 616 (1981).
 - [24] H. O. Meyer et al., *Phys. Rev. C* **37**, 544 (1988).
 - [25] M. Hugi, W. Bauhoff, and H. O. Meyer, *Phys. Rev. C* **28**, 1 (1983).
 - [26] K. H. Hicks et al., *Phys. Rev. C* **38**, 229 (1988).
 - [27] H. V. von Geramb, K. Amos, R. Sprickmann, K. T. Knöpfle, M. Rogge, D. Ingham, and C. Mayer-Böricke, *Phys. Rev. C* **12**, 1697 (1975).
 - [28] E. Colombo et al., *J. Phys. Soc. Japan*, suppl. **44**, 543 (1978).
 - [29] M. C. Munro (1991), ph.D Thesis, University of Melbourne (unpublished).
 - [30] D. K. Hasell, N. E. Davison, T. N. Nasr, B. T. Murdoch, A. M. Sourkes, and W. T. H. van Oers, *Phys. Rev. C* **27**, 482 (1983).

- [31] P. Schwandt, H. O. Meyer, W. W. Jacobs, A. D. Bacher, S. E. Vigdor, M. D. Kaitchuck, and T. R. Donoghue, Phys. Rev. C **26**, 55 (1982).
- [32] S. Dahlgren, check, et al., Nucl. Phys. **A90**, 673 (1967).
- [33] C. Olmer et al., Phys. Rev. C **29**, 361 (1984).
- [34] Q. Chen, J. J. Kelly, P. P. Singh, M. C. Radhakrishna, W. P. Jones, and H. Nann, Phys. Rev. C **41**, 2514 (1990).
- [35] E. E. Gross, R. H. Bassel, L. N. Blumberg, B. J. Morton, A. V. der Woude, and A. Zucker, Nucl. Phys. **A102**, 673 (1967).
- [36] A. Nadasen, P. Schwandt, P. P. Singh, W. W. Jacobs, A. D. Bacher, P. T. Debevec, M. D. Kaitchuck, and J. T. Meek, Phys. Rev. C **23**, 1023 (1981).
- [37] H. Seifert et al., Phys. Rev. C **47**, 1615 (1993).